

1 *Supporting Information for*
2 **System efficiency and power: the bridge between the device and**
3 **system of thermoelectric power generator**

4 Kang Zhu^{1,2}, Biao Deng^{1,2}, Pengxiang Zhang^{1,2}, Hee Seok Kim³,
5 Peng Jiang⁴ and Weishu Liu^{1,2*}

6 ¹ Department of Materials Science and Engineering, Southern University of Science and Technology, Shenzhen,
7 Guangdong 518055, China

8 ² Shenzhen Engineering Research Center for Novel Electronic Information Materials and Devices, Southern
9 University of Science and Technology, Shenzhen, Guangdong 518055, China

10 ³ Department of Mechanical Engineering, University of South Alabama, Mobile, Alabama 36688, USA

11 ⁴ State Key Laboratory of Catalysis, CAS Center for Excellence in Nanoscience, Dalian Institute of Chemical
12 Physics, Chinese Academy of Sciences, Dalian, Liaoning 116023, China

13 *Email: liuws@sustech.edu.cn

14

15 **1. Derivation of the Governing Equation of a Thermoelectric Process**

16 The earlier works by Callen¹ and Domenicali² are reviewed, to present a complete derivation
17 of the differential equation which governs the temperature distribution in a thermoelectric leg in
18 steady state. The particle current density, the energy current density and the entropy current
19 density within a TE leg are respectively denoted as \vec{J} , \vec{W} and \vec{S} . The heat current density is by
20 definition written as $\vec{q} = T\vec{S}$. In a steady-state process the following conditions should be met,

21 $\nabla \cdot \vec{W} = 0 \#(S1)$

22 $\nabla \cdot \vec{J} = 0 \#(S2)$

23 $\nabla \cdot \vec{S} = \dot{S} \#(S3)$

24 where \dot{S} is the entropy production rate per unit volume. The energy current density consists of
25 two parts, i.e., the kinetic part and the potential part, which gives

26 $\vec{W} = \vec{q} + \mu\vec{J} = T\vec{S} + \mu\vec{J} \#(S4)$

27 where $\mu = \mu_c + \mu_e$ is the electrochemical potential energy per particle, with μ_c and μ_e respectively
28 representing the chemical portion and the electrical portion. Under this circumstance the chemical
29 portion is minor and is thus neglected in the following derivations. The electrical part could be
30 written as $\mu_e = e\varphi$, with e being the charge on a particle and φ the electrostatic potential.

31 The entropy production rate is obtained by Eqs. (S1)-(S4) as

32 $S = \nabla \cdot \frac{1}{T} \cdot \vec{W} - \nabla \cdot \frac{\mu}{T} \cdot \vec{J} = \nabla \cdot \frac{1}{T} \cdot \vec{q} - \frac{1}{T} \nabla \mu \cdot \vec{J} \#(S5)$

33 Taking $-\vec{J}$ and \vec{q} as currents, and $\frac{1}{T} \nabla \mu$ and $\frac{1}{T}$ as the driving forces, the relationships between
34 the currents and forces could be written as

$$\begin{cases} -\vec{j} = L_{11}\frac{1}{T}\nabla\mu + L_{12}\nabla\frac{1}{T} \\ \vec{q} = L_{21}\frac{1}{T}\nabla\mu + L_{22}\nabla\frac{1}{T} \end{cases} \#(S6)$$

2 Onsager's theorem³ states that a reciprocal relation, in the form of $L_{12} = L_{21}$ in a two-flow
3 system, exists when there is no magnetic field or Coriolis force. Then Eq. (S6) could be rewritten
4 as

$$\begin{cases} -\vec{j} = L_{11}\frac{1}{T}\nabla\mu + L_{12}\nabla\frac{1}{T} \\ \vec{q} = L_{12}\frac{1}{T}\nabla\mu + L_{22}\nabla\frac{1}{T} \end{cases} \#(S7)$$

6 The kinetic coefficients (L_{11} , L_{12} and L_{22}) are involved with the physical properties (α , σ and
7 κ) of the medium, and are derived as follows. First of all, the thermal conductivity is defined as the
8 heat current density per unit temperature gradient for zero particle current. Keep in mind that the
9 heat current is in the opposite direction of the temperature gradient,

$$\kappa = -\frac{\vec{q}}{\nabla T} \#(S8)$$

11 Based on Eq. (S7) and the zero particle current condition, i.e., $\vec{j} = 0$, the thermal conductivity
12 could be derived as

$$\kappa = \frac{L_{11}L_{22} - L_{12}^2}{T^2L_{11}} \#(S9)$$

14 Secondly, the electrical conductivity is defined as the electric current density ($\vec{j}_e = e\vec{j}$) per unit
15 potential gradient under an isothermal condition. Also keep in mind that the electric current is in
16 the opposite direction of the electrical potential gradient,

$$\sigma = -\frac{e\vec{j}}{\nabla\varphi} \#(S10)$$

18 Again, by Eq. (S7), $\mu_e = e\varphi$, and the isothermal condition, i.e., $\nabla T = 0$, the electrical
19 conductivity could be derived as

$$\sigma = \frac{e^2L_{11}}{T} \#(S11)$$

21 Eliminating the $\nabla\mu$ term in Eq. (S7), the entropy current density could be written as

$$\vec{S} = \frac{\vec{q}}{T} = -\frac{L_{12}}{TL_{11}}\vec{j} + \frac{L_{11}L_{22} - L_{12}^2}{TL_{11}}\nabla\frac{1}{T} \#(S12)$$

23 In Eq. (S12), the first term in the right hand side represents the entropy flow caused by the

24 particle flow, hence the term $-\frac{L_{12}}{TL_{11}}$ means the entropy flow per particle (S_J), which is in a
25 relationship with the Seebeck coefficient by

$$S_J = -\frac{L_{12}}{TL_{11}} = e\alpha \#(S13)$$

27 The kinetic coefficients could be obtained by solving Eqs. (S9), (S11) and (S13),

$$\left\{ \begin{array}{l} L_{11} = \frac{T\sigma}{e^2} \\ L_{12} = -\frac{T^2}{e^2}\sigma S_j = -\frac{T^2}{e}\sigma\alpha \#(S14) \\ L_{22} = \frac{T^3}{e^2}\sigma S_j^2 + T^2\kappa = T^3\sigma\alpha^2 + T^2\kappa \end{array} \right.$$

1 Taking the kinetic coefficients back into Eq. (S7), formulas of the particle current density and
2 heat current density are derived as

$$\left\{ \begin{array}{l} \vec{j} = -\frac{\sigma}{e^2}\nabla\mu - \frac{\sigma\alpha}{e}\nabla T \#(S15) \\ \vec{q} = T\alpha e\vec{j} - \kappa\nabla T \end{array} \right.$$

3 The zero divergence of the energy current density (Eq.(S1)) and the particle current density
4 (Eq. (S2)) lead to

$$\nabla \cdot \vec{q} = -\nabla\mu \cdot \vec{j} \#(S16)$$

5 Substituting Eq. (S15) into Eq. (S16) gives the governing equation as

$$\nabla \cdot (\kappa\nabla T) + \frac{e^2 J_e^2}{\sigma} - eT\nabla\alpha \cdot \vec{j} = 0 \#(S17)$$

6 Taking the electrical current density ($\vec{j}_e = e\vec{j}$) into Eq. (S17),

$$\nabla \cdot (\kappa\nabla T) + \frac{J_e^2}{\sigma} - T\nabla\alpha \cdot \vec{j}_e = 0 \#(S18)$$

7 In a homogeneous medium, Eq. (S18) could be rewritten as

$$\nabla \cdot (\kappa\nabla T) + \frac{J_e^2}{\sigma} - \tau\vec{j}_e \cdot \nabla T = 0 \#(S19)$$

8 where $\tau = T\frac{d\alpha}{dT}$ is the Thomson coefficient. In case of temperature independent physical properties
9 and one-dimension energy flow, Eq. (S19) degrades into a simpler form as

$$\kappa\frac{d^2T}{dx^2} + \frac{J_e^2}{\sigma} = 0 \#(S20)$$

10 2. Derivation of the Maximum Efficiency and Power Formula

11 The analytical solution of the governing equation and boundary conditions (Eq. (5)) leads to
12 a temperature profile of the TEG leg as

$$\left\{ \begin{array}{l} T = -\frac{0.5I^2RR_{t,l}}{L^2}x^2 + C_1x + C_2 \\ C_1 = \frac{1c_1f_cI^2RR_{t,l} + 0.5c_1c_2I^2RR_{t,l} + \alpha R_{t,l}I(f_hT_c + f_cT_h) - \Delta T}{f_h + f_c + c_1c_2} \\ C_2 = \frac{1}{c_1} \left\{ \frac{f_h[c_1f_cI^2RR_{t,l} + 0.5c_1c_2I^2RR_{t,l} + \alpha R_{t,l}I(f_hT_c + f_cT_h) - \Delta T]}{f_h + f_c + c_1c_2} + T_h \right\} \\ c_1 = 1 + f_h\alpha R_{t,l}I \\ c_2 = 1 - f_c\alpha R_{t,l}I \end{array} \right. \#(S21)$$

13 where R denotes the electric resistance of the TEG leg. From the above equation the leg terminal
14 temperatures and effective temperature difference are given by

$$\left\{ \begin{array}{l} T_h' = C_2 \\ T_c' = -0.5I^2RR_{t,l} + C_1L + C_2 \\ \Delta T' = \frac{\Delta T - \alpha R_{t,l}I(f_hT_c + f_cT_h + f_hf_cI^2RR_{t,l}) + 0.5I^2RR_{t,l}(f_h - f_c)}{f_h + f_c + c_1c_2} \end{array} \right\} \#(S22)$$

From the equation of $\Delta T'$, the contributions of the external thermal resistances, the Peltier effect and the Joule effect to the effective temperature difference across the TEG leg could be clearly clarified. Among these factors, the external thermal resistances will definitely decrease $\Delta T'$ as exhibited by the division of ΔT by $f_h + f_c$. Since the Peltier effect absorbs heat from the hot side and releases heat to the cold side, it acts to lower T_h' and raise T_c' , leading to a further reduction in $\Delta T'$, reflected by the negative sign before the Peltier term (the second term in the numerator). With regard to the Joule effect (the third term in the numerator), it acts primarily to raise the temperature level of the whole leg rather than only influence some specific regions, so its contribution to $\Delta T'$ is generally trivial compared to other factors.

According to the relationship between the electric current and the effective temperature difference $\Delta T'$, i.e.,

$$I = \frac{\alpha \Delta T'}{R(1+m)} \#(S23)$$

a cubic equation of the electric current is deduced as

$$\left\{ \begin{array}{l} b_0I^3 + b_1I^2 + b_2I + b_3 = 0 \\ b_0 = f_hf_c\alpha^2R_{t,l}^2Rm \\ b_1 = -\alpha R_{t,l}R(f_h - f_c)(m + 0.5) \\ b_2 = -[\alpha^2R_{t,l}(f_hT_c + f_cT_h) + (1 + f_h + f_c)(1 + m)R] \\ b_3 = \alpha \Delta T' \end{array} \right\} \#(S24)$$

where m is the ratio of the load resistance to the TE leg electrical resistance. Unfortunately, even though the analytical solutions of a cubic equation do exist, the complicated formation of Eq.(S24) will eventually make the analytical derivations of maximum power output and conversion efficiency unattainable. To make a balance between precision and concision (and also feasibility), it is necessary to eliminate or simplify some terms within the temperature profile Eq.(S21) carefully. Besides, the original equations of (S21), (S22) and (S24) could be packaged into a computational program to generate exact numerical solutions, serving as reference data for the validation of the simplified analytical model.

First of all, as an attempt to neglect the influence of Joule effect on the effective temperature difference, the terms including I^2R in Eq.(S1) are eliminated, resulting in a simplified temperature profile as

$$\left\{ \begin{array}{l} T = C_1x + C_2 \\ C_1 = \frac{1\alpha R_{t,l}I(f_hT_c + f_cT_h) - \Delta T}{L(f_h + f_c + c_1c_2)} \\ C_2 = \frac{f_hT_c + f_cT_h + c_2T_h}{f_h + f_c + c_1c_2} \\ c_1 = 1 + f_h\alpha R_{t,l}I \\ c_2 = 1 - f_c\alpha R_{t,l}I \end{array} \right\} \#(S25)$$

Secondly, the terms c_1 and c_2 are checked for any chance of simplification, since their

1 multiplication in the denominator of C_1 and C_2 will continue to generate a cubic equation of I ,
 2 which is still difficult to solve analytically. At first sight, the Seebeck coefficient is generally on the
 3 order of 10^{-4} V/K, thus the terms $f_h \alpha R_{t,l} I$ and $f_c \alpha R_{t,l} I$ are liable to be of small values. Furthermore,
 4 any rise in the thermal resistance ratios will lead to a drop of I , making the second terms in C_1 and
 5 C_2 self-confined to minor values compared to 1. Therefore, C_1 and C_2 are simplified to 1 for further
 6 derivation, and the final temperature profile equation is written as

$$7 \quad \begin{cases} T = C_1 x + C_2 \\ C_1 = \frac{1 \alpha R_{t,l} I (f_h T_c + f_c T_h) - \Delta T}{L (1 + f_h + f_c)} \quad \#(S26) \\ C_2 = \frac{T_h + f_h T_c + f_c T_h}{1 + f_h + f_c} \end{cases}$$

8 The validity of the above simplifications will be checked in the following section. The leg
 9 terminal temperatures and effective temperature drop are once again deduced as

$$10 \quad \begin{cases} T'_h = C_2 \\ T'_c = C_1 L + C_2 \\ \Delta T' = \frac{\Delta T - \alpha R_{t,l} I (f_h T_c + f_c T_h)}{1 + f_h + f_c} \quad \#(S27) \end{cases}$$

11 and the electric current is in the form of

$$12 \quad \begin{cases} I = \frac{1}{1 + f_h + f_c} \frac{\alpha \Delta T}{R} \frac{1}{m + 1 + ZT^*} \\ T^* = \frac{f_h T_c + f_c T_h}{1 + f_h + f_c} \quad \#(S28) \end{cases}$$

13 The output power of the TEG leg is then given by

$$14 \quad P = I^2 R m = \frac{1}{(1 + f_h + f_c)^2} \frac{(\alpha \Delta T)^2}{R} \frac{m}{(m + 1 + ZT^*)^2} \quad \#(S29)$$

15 From Eq.(S9) the maximum output power per leg area is achieved in the form of

$$16 \quad w_{max} = \frac{1}{(1 + f_h + f_c)^2} \frac{(\Delta T)^2}{4L} \frac{\alpha^2 \sigma}{1 + ZT^*} \quad \#(S30)$$

17 when

$$18 \quad m_{opt,w} = 1 + ZT^* \quad \#(S31)$$

19 The heat absorption rate at the hot side of the TEG leg is given by

$$20 \quad Q_h = -\kappa A C_1 + \alpha C_2 I = \frac{1}{1 + f_h + f_c} \frac{\Delta T}{R_{t,l}} \left(1 + \frac{1}{1 + f_h + f_c} \frac{ZT_h}{m + 1 + ZT^*} \right) \quad \#(S32)$$

21 Thus the conversion efficiency is evaluated to be

$$22 \quad \eta = \frac{P}{Q_h} = \frac{Z \Delta T m}{(m + 1 + ZT^*) [(1 + f_h + f_c)(m + 1 + ZT^*) + ZT_h]} \quad \#(S33)$$

23 Letting $d\eta/dm = 0$, an equation of m is obtained as

$$24 \quad m = \sqrt{(1 + ZT^*) [1 + Z(T^* + T_h^*)]} \quad \#(S34)$$

25 where $T_h^* = \frac{T_h}{1 + f_h + f_c}$. This should be the optimum electric resistance ratio to achieve maximum

1 conversion efficiency. However, as the external thermal resistances diminish, Eq. (S34) leads to an
 2 optimum m of $\sqrt{1 + ZT_h}$ for maximum efficiency rather than the expected $\sqrt{1 + Z\bar{T}}$, implying some
 3 deficiency in the derivation mainly caused by the simplifications in Eqs. (S25) and (S26).
 4 Considering this, here we make a minor correction on Eq. (S34) to obtain a self-justifying
 5 expression as

$$6 \quad m_{opt,\eta} = \sqrt{(1 + ZT^*)[1 + Z(T^* + \bar{T}^*)]} \quad \#(S35)$$

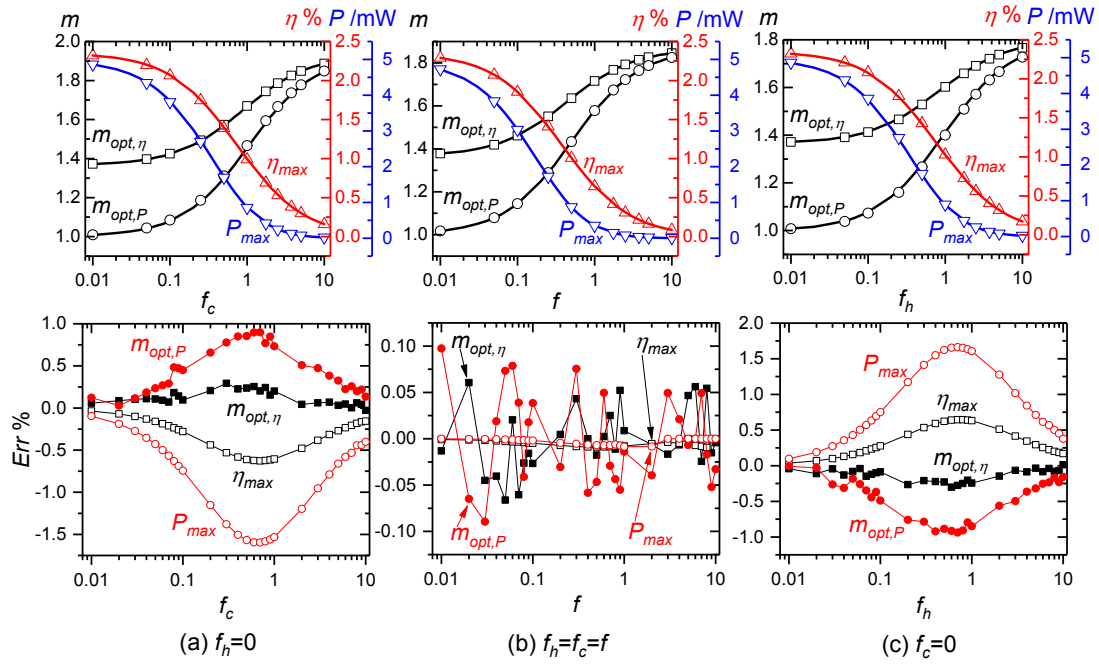
7 where $T^* = \frac{\bar{T}}{1 + f_h + f_c}$. It is found to give a better evaluation of the optimum condition and
 8 generate a concise formula of maximum conversion efficiency as follows,

$$9 \quad \left\{ \begin{array}{l} \eta_{max} = \frac{\Delta T}{T_h} \frac{m_{opt,\eta} - 1}{m_{opt,\eta} + \frac{T_c}{T_h} + \beta} \quad (a) \\ \beta = 2 \frac{T^* \bar{T}}{T^* T_h} m_{opt,\eta} \left(1 + \frac{m_{opt,\eta}}{1 + ZT^*} \right) \quad (b) \end{array} \right. \quad \#(S36)$$

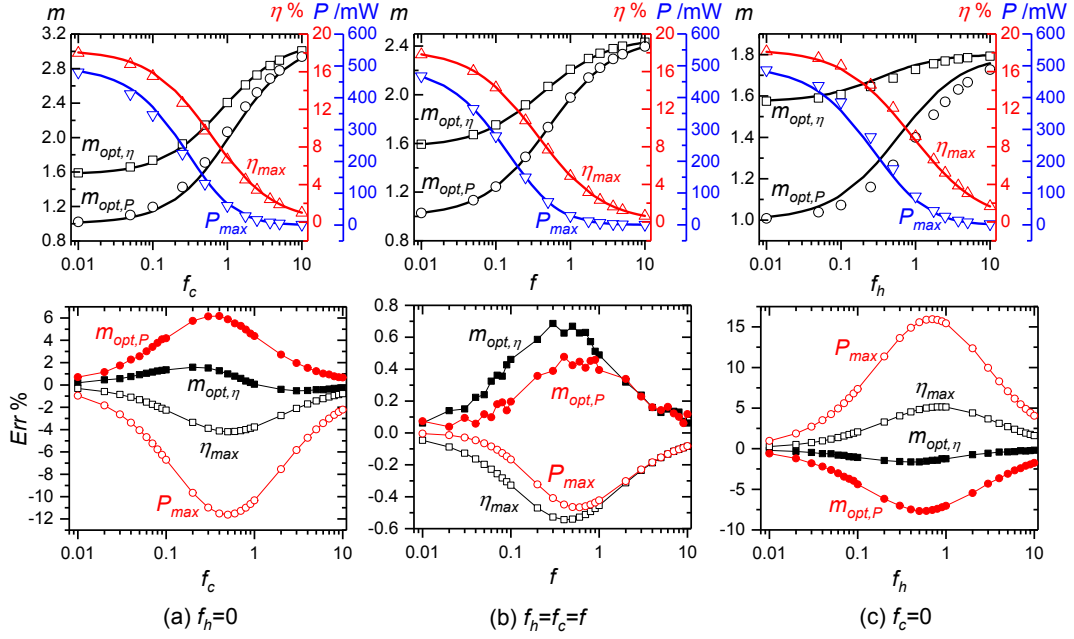
10 The formulas in Eq.(S30-S31) and (S35-S36) lead to evaluations of maximum conversion
 11 efficiency and power output of a TEG system in finite external thermal resistance situations, as
 12 well as their corresponding electrical conditions.

13 3. Validation of the TEG Model

14 To check the accuracy of the explicit formulas of maximum conversion efficiency and power
 15 output, the calculated values by Eqs.(S30) and (S36) as well as the corresponding electrical
 16 resistance ratios by Eqs.(S31) and (S35) are compared with exact results from a peak search
 17 program based on the numerical solutions of Eqs. (S21), (S22) and (S24), under a total temperature
 18 difference of 50 K and a heat sink temperature of 300 K, as shown in Fig. S1. The thermal resistance
 19 ratio range (0.01~10) adopted in the validation covers most realistic thermal conditions for TEGs
 20 as illustrated in the main part. Three different cases of external thermal resistance distribution are
 21 considered, among which the two asymmetric cases with zero external thermal resistance at one
 22 side of the TE module but finite thermal resistance at the other side represent two boundaries of
 23 the realistic asymmetric conditions, while the symmetric case with equal thermal resistances at
 24 the two sides is a special condition occasionally occurs in practical applications. It can be seen that
 25 the derived formulas can precisely evaluate the optimum operating points.



1
2 Fig. S1 Optimum operating states of a TEG, $\Delta T = 50 K$ (In the upper row, solid line: numerical
3 results; discrete points: analytical evaluations. The lower row presents relative errors)
4 More specifically, the formulas can achieve a relative error band of $\pm 0.75\%$ for maximum
5 conversion efficiency ($\pm 0.5\%$ for $m_{opt,\eta}$) and $\pm 1.75\%$ for maximum power output ($\pm 1\%$ for $m_{opt,P}$)
6 respectively under asymmetric thermal resistance distributions. The evaluation precisions are
7 even better under symmetric thermal resistance distributions with all error bands within $\pm 0.1\%$.
8 Hence we can declare that the derived formulas are competent to give satisfying evaluations of a
9 TEG's optimum operating states in terms of both efficiency and power output, under moderate
10 total temperature differences of tens of degrees and whatever external heat transfer conditions.
11 To check the formulas for wider applications with higher temperature ranges, a similar
12 comparison is made under a total temperature difference of 500 K, as shown in Fig. S2. At first
13 sight of the upper row in the figure, the analytical evaluations generally follow the evolutions of
14 numerical solutions versus thermal resistance ratios under different distributions. Meanwhile,
15 some deviations between the discrete points and solid lines can be clearly seen, particularly for
16 the maximum power output states under asymmetric thermal resistance distributions. From the
17 error curves in the lower row, under asymmetric distributions with zero thermal resistance at the
18 hot side (Fig. S2(a)), the maximum conversion efficiency and power output of the system are
19 underestimated with relative error bands of $-5\% \sim 0\%$ and $-12\% \sim 0\%$, respectively. Under the
20 opposite asymmetric distributions (Fig. S2(c)), the maximum conversion efficiency and power
21 output of the system are overestimated with relative error bands of $0\% \sim 5\%$ and $0\% \sim 16\%$,
22 respectively. While under symmetric thermal resistance distributions (Fig. S2(b)), the explicit
23 formulas continue to give rather accurate evaluations of all the optimum operating states with
24 relative error bands within $\pm 0.8\%$.



1

2 Fig. S2 Optimum operating states of a TEGS, $\Delta T = 500 K$ (In the upper row, solid line: numerical
3 results; discrete points: analytical evaluations. The lower row presents relative errors)

4 This distinction could be explained by an inspection on Eq.(S25). Keep in mind that we have
5 simplified c_1 and c_2 to 1 for further derivation. Under symmetric thermal resistance distributions,
6 the original c_1 and c_2 would be a little larger and smaller than 1 respectively, thus a multiplication
7 of them could offset the deviations for each other and make the simplification more confident.
8 Besides, the most significant errors are always found to occur within a range of 0.2~2 for the
9 thermal resistance ratios, which is a consequence of a trade-off between the thermal resistance
10 ratio and the electrical current included in c_1 and c_2 . In summary, for a higher available
11 temperature difference of 500 K, the derived formulas can lead to conversion efficiency
12 evaluations within an accuracy of $\pm 5\%$ for all kinds of thermal resistance distributions and levels,
13 while significant deviations over 15% arise when assessing the maximum power output for partial
14 ranges of thermal resistance ratios under asymmetric distributions, thus some kind of modification
15 of the power output formula is essential for a higher precision.

16 4. Modification of the TEG Model

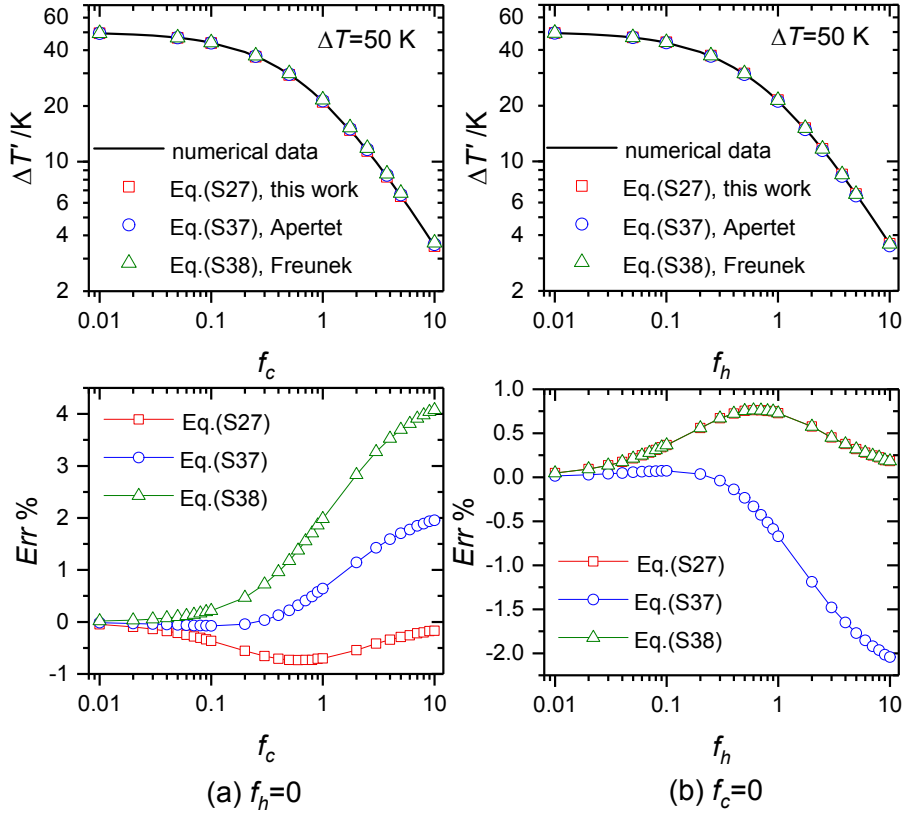
17 To modify the power output formula, we should firstly go back to the effective temperature
18 difference equation (S27), whose accuracy directly affects the power output evaluation. Two
19 existing calculating formulas for the effective temperature difference from the literature (Refs. 4
20 and 5) based on the effective thermal conductance concept are also given here for comparison,
21 using currently adopted nomenclatures after some equivalent transformations,

$$22 \Delta T' = \frac{\Delta T - \alpha R_{t,l} I (f_h + f_c) \bar{T}}{1 + f_h + f_c} \#(S37)$$

$$23 \Delta T' = \frac{\Delta T - \alpha R_{t,l} I (f_h + f_c) T_c}{1 + f_h + f_c} \#(S38)$$

24 It can be clearly seen that these two models do not make any distinction between the hot

1 and cold side thermal resistances, since the external thermal resistance ratios always appear in a
 2 sum, which is in consistency with the statement of Stevens⁶ on the indiscriminate effect of external
 3 thermal resistance at either side under limited temperature difference conditions. Consequently,
 4 both Eqs. (S37) and (S38) are expected to give accurate estimations of effective temperature
 5 differences under a moderate total temperature difference of 50 K, as shown in Fig. S3. Also
 6 presented in the figure are the evaluations by our model (Eq. (S27)) and exact numerical data.



7

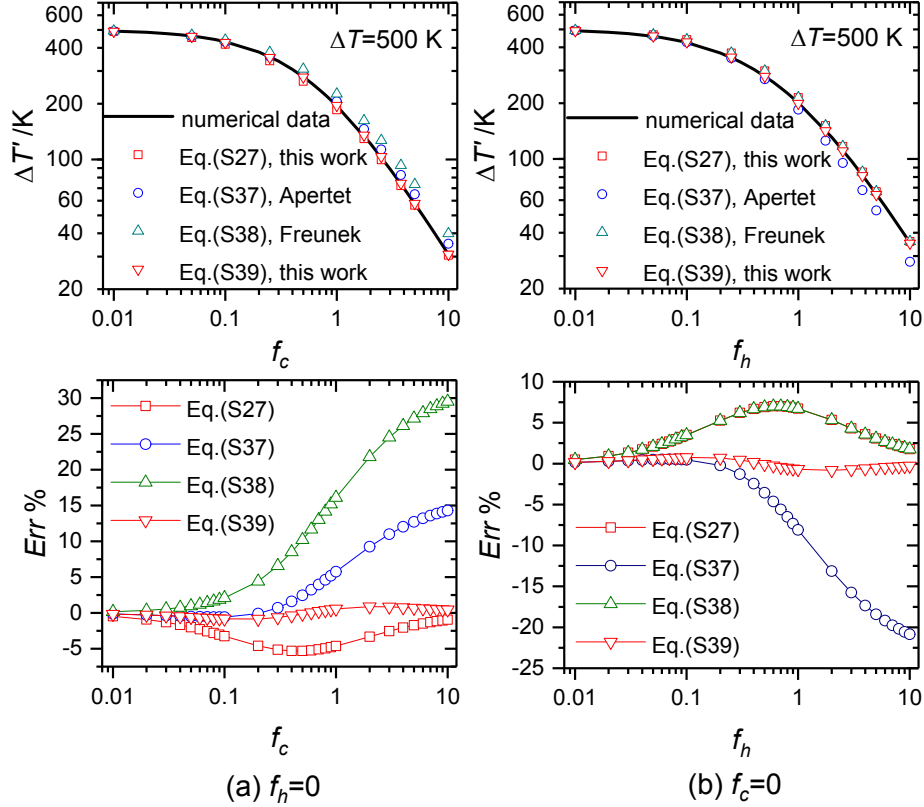
8 Fig. S3 Effective temperature differences for maximum power output, $\Delta T = 50 K$

9 Under asymmetric distributions with zero thermal resistance at the hot side, Freunek's model
 10 (Eq. (S38)) leads to the highest relative error among the three models, with a peak (but still rather
 11 low) value of 4% at $f_c = 10$. While under the opposite asymmetric distributions, Apertet's model
 12 (Eq. (S37)) leads to a peak value of -2% at $f_h = 10$. As a whole, our original model (Eq. (S27)) results
 13 in the best evaluation of effective temperature differences for maximum power output under
 14 different thermal resistance distributions. In fact, if $f_c = 0$, our model and Freunek's model turn
 15 to become the same one. In addition, if $f_h = f_c$, then our model and Apertet's model turn to be
 16 the same. Therefore, these formulas could be regarded as variants to each other with different
 17 aspects of simplification, and when combining two or three of the above formulas, a new one with
 18 higher accuracy throughout the whole range may be found.

19 Revisiting the error curves in Fig. S3, it is noted that Eq. (S37) exhibits outstanding
 20 performance before f_c or f_h reaches 0.2 and turns to degrade thereafter. As for Eq. (S27), it only
 21 behaves not well within a thermal resistance ratio range of 0.2~2. Moreover, the error curves of
 22 Eqs. (S27) and (S37) present opposite varying trends within most part of the specific range (0.2~2),
 23 hence a weighted summation is carried out between these two formulas, with a weight ratio of
 24 $f_h + f_c$ for Eq. (S27) and 1 for Eq. (S37), resulting in a new formula written as

$$\Delta T' = \frac{\Delta T}{1 + f_h + f_c} - \frac{\alpha R_{t,l}(f_h + f_c)[T + (f_h T_c + f_c T_h)]}{(1 + f_h + f_c)^2} \quad \#(S39)$$

This new formula is expected to remove the wave peak of the error curve of Eq.(S27) without affecting its good performance in other ranges by the filter effect of the weight allocation. To validate this expectation, the effective temperature differences for maximum power output are evaluated by Eq. (S39) as well as the former three formulas under a total temperature difference of 500 K, and the analytical results are compared with numerical solutions, as shown in Fig. S4.



7

8 Fig. S4 Effective temperature differences for maximum power output, $\Delta T = 500$ K

9 As expected, the applications of Eqs. (S37) and (S38) under a higher temperature difference
10 lead to significant deviations within a big portion of the commonly encountered thermal resistance
11 ratio range, particularly for higher ratios. The peak relative errors of Eqs. (S37) and (S38) are
12 around -20% and 30%, respectively. The error band of our original model (Eq. (S27)) covering all of
13 the evaluated conditions is -5%~7%, which is much better than those of Eqs. (S37) and (S38) due
14 to the abandon of the constant heat flow assumption within the whole system. In comparison, the
15 new formula in Eq. (S39) gives excellent evaluations throughout the whole range within an error
16 band of $\pm 1\%$.

17 Based on Eq. (S39), a new formula of the power output is derived as

$$P = \frac{1}{(1 + f_h + f_c)^2} \frac{(\alpha \Delta T)^2}{R} \frac{m}{\left[m + 1 + \frac{f_h + f_c}{1 + f_h + f_c} Z(T^* + T^*) \right]^2} \quad \#(S40)$$

18

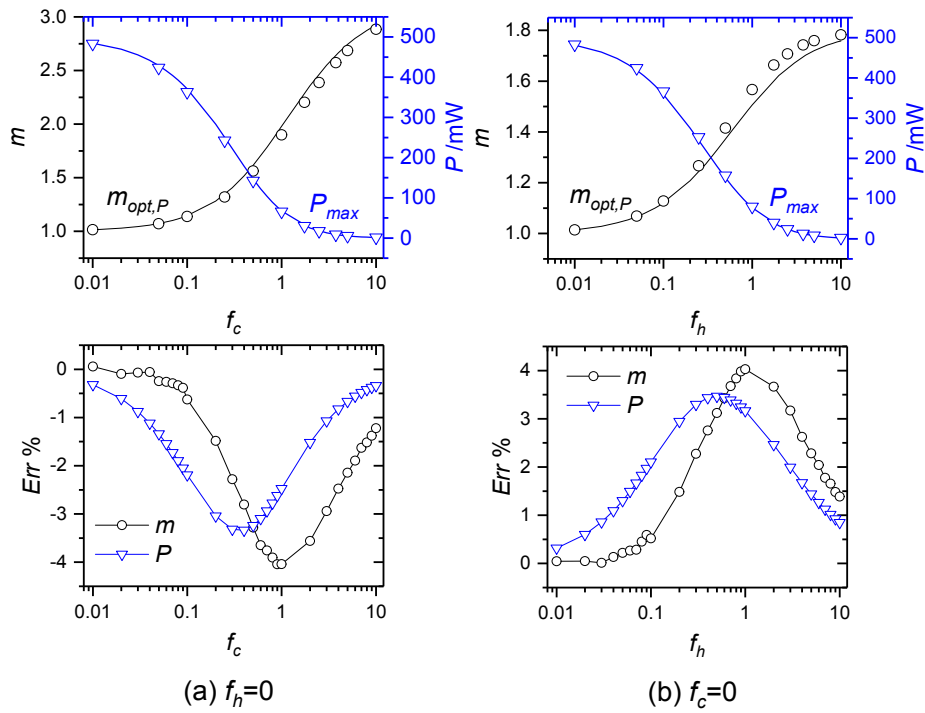
19 and the maximum power output per leg area is achieved when

$$m_{opt,w} = 1 + \frac{f_h + f_c}{1 + f_h + f_c} Z(T^* + T^*) \quad \#(S41)$$

1 as

$$w_{max} = \frac{1}{(1 + f_h + f_c)^2} \frac{\Delta T^2}{4Lm_{opt,w}} \alpha^2 \sigma \quad \#(S42)$$

4 The evaluation capabilities of Eqs. (S41) and (S42) are checked for asymmetric thermal
5 resistance distributions, as shown in Fig. S5. Remarkable advances in evaluations of both the
6 optimum electrical resistance ratio and the maximum power output are achieved with an error
7 band of $\pm 4\%$ for both of them. In symmetric distributions, the effective temperature difference
8 equations (S27) and (S39) are actually equivalent to each other, so the good evaluation capability
9 for symmetric thermal resistance distributions is also retained in the new power output formulas.



10

11 Fig. S5 Maximum power points obtained by the revised formulas Eqs. (S41-42), $\Delta T = 500 K$

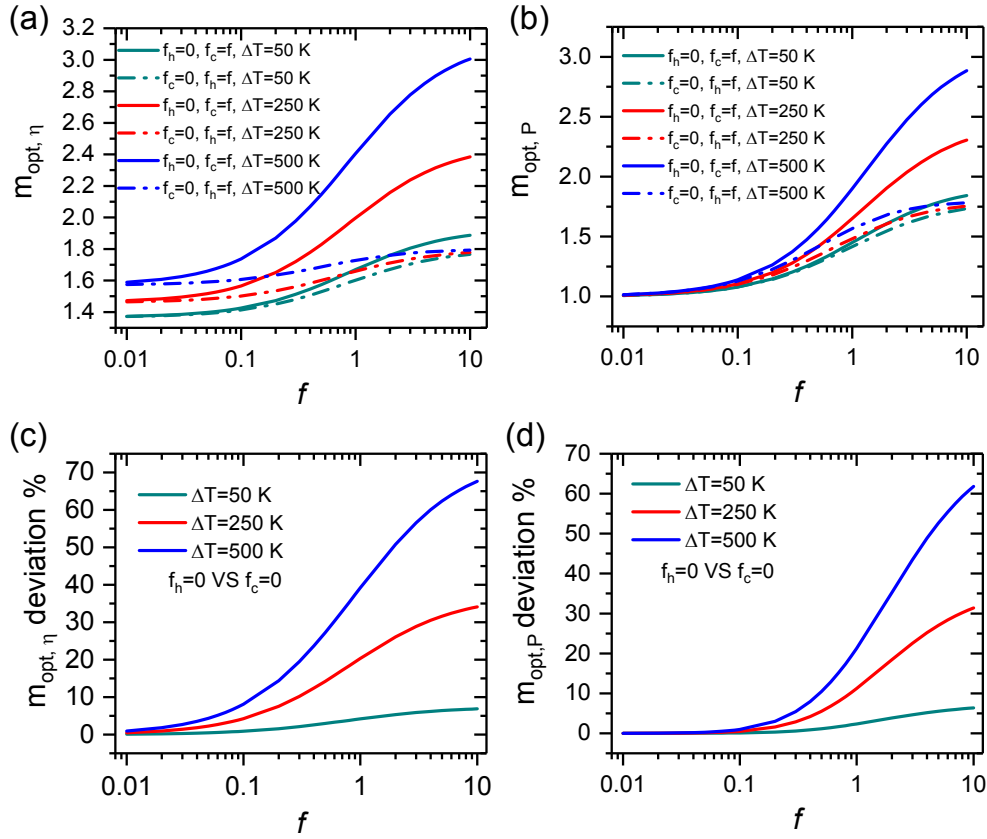
12 Finally, we obtain a set of explicit formulas to conveniently and accurately evaluate the
13 optimum conversion efficiency and power output points for a TEGS working in realistic thermal
14 environments, with relative deviations no higher than 5% over wide ranges of total temperature
15 difference and thermal resistance distribution. The formulas are rewritten here as

$$\left\{ \begin{array}{l} \eta_{max} = \frac{\Delta T}{T_h} \frac{m_{opt,\eta} - 1}{m_{opt,\eta} + \frac{T_c}{T_h} + \beta} \quad (a) \\ m_{opt,\eta} = \sqrt{(1 + ZT^*) [1 + Z(T^* + T^*)]} \quad (b) \quad \#(S43) \\ w_{max} = \frac{1}{(1 + f_h + f_c)^2} \frac{\Delta T^2}{4Lm_{opt,w}} \alpha^2 \sigma \quad (c) \\ m_{opt,w} = 1 + \frac{f_h + f_c}{1 + f_h + f_c} Z(T^* + T^*) \quad (d) \end{array} \right.$$

16

1 where $T^* = \frac{f_h T_c + f_c T_h}{1 + f_h + f_c}$, $T^* = \frac{\bar{T}}{1 + f_h + f_c}$, and $\beta = 2 \frac{T^* \bar{T}}{\bar{T}^* T_h} m_{opt,\eta} \left(1 + \frac{m_{opt,\eta}}{1 + ZT^*} \right)$.

2 5. Effect of the thermal resistance distribution



3
4 Fig. S6 (a) Evolution curves of the optimum electrical resistance matching parameter for
5 maximum system efficiency for two critical thermal resistance distributions, one with zero
6 thermal resistance at the hot side, and the other with zero thermal resistance at the cold side; (b)
7 Evolution curves of the optimum electrical resistance matching parameter for maximum output
8 power for two critical thermal resistance distributions; (c) and (d), Deviations of the optimum
9 electrical resistance matching parameters between two critical thermal resistance distributions,
10 for maximum system efficiency and output power respectively

11 6. On the design of TEGs with limited ΔT

12 Denoting the heat transfer coefficients at the hot and cold sides as h_h and h_c , and the fill factor
13 as FF , the thermal resistance ratios can be expressed as

14 $f_h = \frac{FF \cdot \kappa}{h_h L}$, $f_c = \frac{FF \cdot \kappa}{h_c L}$, $F = \frac{FF \cdot \kappa}{hL}$ # (S44)

15 where $\frac{1}{h} = \frac{1}{h_h} + \frac{1}{h_c}$.

16 Substituting Eq. (S44) into Eq. (S43(c)-(d)), the maximum power output is rewritten as

$$P_{max} = \frac{Z\Delta T^2 A}{4} \frac{1}{\frac{L}{\kappa} + \frac{\kappa(F\bar{F})^2}{L} \left[1 + hZ \left(\frac{T_c}{h_h} + \frac{T_h}{h_c} \right) \right] + \frac{FF}{h} (2 + Z\bar{T})} \quad \#(S45)$$

The power density based on the substrate area is then derived as

$$P_{dens} = \frac{1}{4} Z\Delta T^2 \frac{1}{\frac{L^*}{\kappa} + \frac{\kappa}{L^*} \left(\frac{1}{h} \right)^2 \left[1 + hZ \left(\frac{T_c}{h_h} + \frac{T_h}{h_c} \right) \right] + \frac{1}{h} (2 + Z\bar{T})} \quad \#(S46)$$

where $L^* = \frac{L}{FF}$, and it could be used as a lumped dimension parameter for the geometry of the TE legs. The maximum power density is achieved by equating the former two terms in the denominator, which leads to

$$L^* = \frac{\kappa}{h} \sqrt{1 + hZ \left(\frac{T_c}{h_h} + \frac{T_h}{h_c} \right)} \quad \#(S47)$$

When the effective temperature difference is small, $\frac{T_h'}{T_c'}$ is close to 1. An approximation could be made based on the Taylor expansion and by neglecting higher order terms as

$$\left(\frac{T_h'}{T_c'} \right)^{kg} \cong 1 + kg \left(\frac{T_h'}{T_c'} - 1 \right) \quad \#(S48)$$

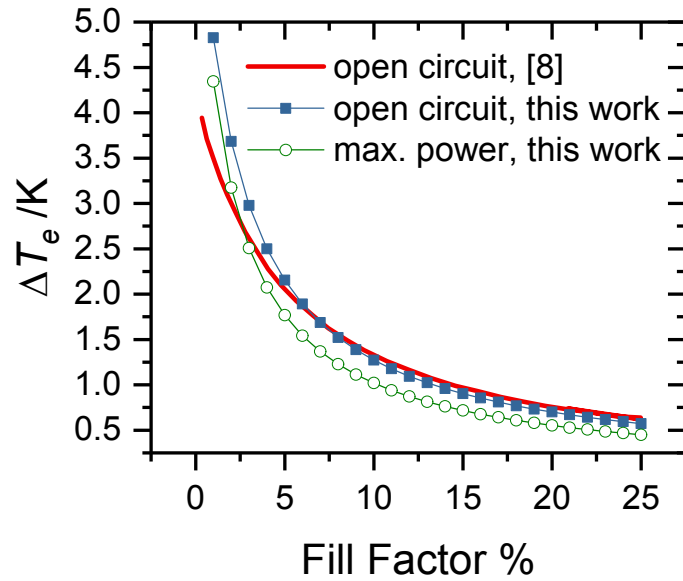
Then the square bracket term in the effective thermal conductivity⁷ is converted into

$$1 - \left(\frac{T_h'}{T_c'} \right)^{kg} \cong kg \left(1 - \frac{T_h'}{T_c'} \right) = \frac{2(\sqrt{1 + z\bar{T}} - 1)T_h' - T_c'}{z\bar{T} T_c'} \quad \#(S49)$$

The effective thermal conductivity is rewritten as

$$\begin{aligned} \kappa_{eff} &= \kappa \sqrt{1 + z\bar{T}} \frac{T_h' \sqrt{1 + z\bar{T}} + 1}{T_h' - T_c'} \cdot \left[1 - \left(\frac{T_h'}{T_c'} \right)^{kg} \right] \quad \#(S50) \\ &\cong \kappa \sqrt{1 + z\bar{T}} \frac{T_h'}{T_c'} \\ &\cong \kappa \sqrt{1 + z\bar{T}} \end{aligned}$$

To validate the analytical model for ignoring relevant side effects including the thermal spreading resistance within the substrate and the thermal shunt effect of air surrounding the TE legs, a comparison on the effective temperature difference under open-circuit condition is carried out between the analytical results and the reported data⁸ following a comprehensive consideration of the involved side effects, as shown in Fig. S6. Good agreements can be seen for fill factors higher than 5%, implying a solid validity of the model for practical applications. Also presented here is the effective temperature difference curve for maximum power output, which is obviously lower than that under the open-circuit condition, once again highlighting the importance of thermal-electrical coupled analysis on the accurate evaluation of the system performance, even in situations with severely limited temperature differences.



1

2

Fig. S7 Effective temperature difference evolutions under open circuit condition and for maximum power versus fill factor of the TEG, a comparison between analytical results obtained in this work and reference data⁸

3

4

5

6

References

7

1 H. B. Callen. The application of Onsager's reciprocal relations to thermoelectric, thermomagnetic, and galvanomagnetic effects. *Physical Review*, 1948, 73(11), 1349-1358.

8

2 C. A. Domenicali. Stationary temperature distribution in an electrically heated conductor. *Journal of Applied Physics*, 1954, 25(10), 1310-1311.

9

3 L. Onsager. Reciprocal relations in irreversible processes. I. *Physical Review*, 1931, 37, 405-426.

10

4 Y. Apertet, H. Ouerdane, O. Glavatskaya, C. Goupil and Ph. Lecoer. Optimal working conditions for thermoelectric generators with realistic thermal coupling. *EPL.*, 2012, 97(2), 28001.

11

5 M. Freunek, M. Muller, T. Ungan, W. Walker and L. M. Reindl. New physical model for thermoelectric generators. *Journal of Electronic Materials*, 2009, 38(7), 1214-1220.

12

6 J. W. Stevens. Optimal design of small ΔT thermoelectric generation systems. *Energy Conversion and Management*, 2001, 42, 709-720.

13

7 L. L. Baranowski, G. J. Snyder and E. S. Toberer. Effective thermal conductivity in thermoelectric materials. *J. Appl. Phys.*, 2013, 113, 204904.

14

8 F. Suarez, A. Nozariasbmarz, D. Vashaee and M. C. Ozturk. Designing thermoelectric generators for self-powered wearable electronics. *Energy Environ. Sci.*, 2016, 9, 2099-2113.

15

16

17

18

19

20

21

22